



**HAL**  
open science

## Guidance of zoospores by potassium gradient sensing mediates aggregation

Eric Galiana, Céline Cohen, Philippe Thomen, Catherine Etienne, Xavier Noblin

► **To cite this version:**

Eric Galiana, Céline Cohen, Philippe Thomen, Catherine Etienne, Xavier Noblin. Guidance of zoospores by potassium gradient sensing mediates aggregation. *Journal of the Royal Society Interface*, 2019, 16 (157), pp.20190367. 10.1098/rsif.2019.0367 . hal-02422674

**HAL Id: hal-02422674**

**<https://hal.science/hal-02422674>**

Submitted on 25 May 2020

**HAL** is a multi-disciplinary open access archive for the deposit and dissemination of scientific research documents, whether they are published or not. The documents may come from teaching and research institutions in France or abroad, or from public or private research centers.

L'archive ouverte pluridisciplinaire **HAL**, est destinée au dépôt et à la diffusion de documents scientifiques de niveau recherche, publiés ou non, émanant des établissements d'enseignement et de recherche français ou étrangers, des laboratoires publics ou privés.



## 1 ABSTRACT

2           The biflagellate zoospores of some phytopathogenic *Phytophthora* species spontaneously  
3 aggregate within minutes in suspension. We show here that *P. parasitica* zoospores can form  
4 aggregates in response to a  $K^+$  gradient with a particular geometric arrangement. Using time-lapse  
5 live imaging in macro- and microfluidic devices, we defined (i) spatiotemporal and concentration-  
6 scale changes in the gradient, correlated with (ii) the cell distribution and (iii) metrics of zoospore  
7 motion (velocity, trajectory). In droplets, we found that  $K^+$ -induced aggregates resulted from a  
8 single biphasic temporal sequence involving negative chemotaxis followed by bioconvection over  
9 a  $K^+$  gradient concentration scale [0-17 mM]. Each  $K^+$ -sensing cell moved into a region in which  
10 potassium concentration is below the threshold range of 1-4 mM, resulting in swarming. Once a  
11 critical population density had been achieved, the zoospores formed a plume that migrated  
12 downward, with fluid advection in its wake and aggregate formation on the support surface. In  
13 the microfluidic device, the density of zoospores escaping potassium was similar to those  
14 achieved in droplets. We discuss possible sources of  $K^+$  gradients in the natural environment  
15 (zoospore population, microbiota, plant roots, soil particles), and implications for the events  
16 preceding inoculum formation on host plants.

17

## 1        **1. Introduction**

2            The genus *Phytophthora*, which belongs to the class Oomycetes, includes some of the  
3 most destructive plant pathogens known, responsible for diseases on crops and in natural  
4 ecosystems worldwide. They grow as filamentous coenocytic hyphae producing various types of  
5 sexual and asexual propagules. In most cases, both dispersal and primary infection are mediated  
6 by airborne sporangia or waterborne zoospores [1, 2]. The zoospores are uninuclear and  
7 reniform, with typical cell body dimensions of 7-10 and 5-7  $\mu\text{m}$  along the antero-posterior and  
8 dorso-ventral axes, respectively. They have a locomotor apparatus consisting of two flagella (10-  
9 20  $\mu\text{m}$ ) inserted into a longitudinal and ventral groove, enabling them to explore aqueous  
10 environments and reach potential hosts. A “tinsel-type” flagellum with lateral mastigonemes  
11 along its entire length beats in front of the cell body. Behind the cell body, there is a smooth  
12 “whiplash-type” flagellum [1, 2].

13            Exogenous signals may bias zoospore motility such that the direction of movement is not  
14 random. Zoospores have sensory systems enabling them to respond to chemical gradients  
15 (chemotaxis), oxygen (aerotaxis), ionic fields (electrotaxis), gravity (negative geotaxis) and light  
16 (phototaxis). They target plant tissues by following gradients of various ions and compounds such  
17 as plant isoflavones, amino acids and sugars [3-5]. For example, *P. palmivora* zoospores display  
18 anodal electrotaxis in electrical fields of at least 0.5 V/m, of similar strength to those found in the  
19 physiological fields around plant roots [6]. When a zoospore reaches a potential infection site,  
20 the cell sheds its flagella, synthesizes a primary cell wall and generates a germ tube that  
21 penetrates the host tissue [1, 7-9].

1 Zoospores can control their motility in response to self-produced signals. They swarm  
2 even in populations composed exclusively of swimming zoospores, and they swim toward  
3 encysted spores, leading to auto-aggregation (autotaxis) [10, 11] or biofilm formation on plant  
4 surfaces [12, 13]. There is evidence to suggest that coordinated zoospore behavior may regulate  
5 plant infection through interspecific or intraspecific cell-to-cell signaling [12, 14]. However, it  
6 remains unclear how zoospores perceive cell density, transduce signals and control their own  
7 auto-aggregation. Mathematical and experimental data indicate that the convective zoospore  
8 movement associated with plume formation and auto-aggregation is consistent with predictions  
9 for bioconvection [15]. Bioconvection has been reported for microorganisms swimming towards  
10 the liquid-air surface and aggregating at the top layer of the suspension. This leads to a higher cell  
11 density at the surface than in the bulk of the fluid. Gravity destabilizes the dense layer of cells  
12 formed at the fluid surface, creating convective plumes. Bioconvection modelling uses cell  
13 concentration in a continuous sense assuming that the cell concentration gradient drives the  
14 instability [16-18]. *P. infestans* zoospores may also display sequential combinations of  
15 bioconvection followed by chemotaxis between plumes [11]. *Phytophthora* zoospores have been  
16 reported to produce and use molecules to monitor cell density but no auto-attractant has been  
17 identified to date. *P. parasitica* zoospores produce an AI-2-like signal (but not N-acyl homoserine  
18 lactones) that could drive quorum sensing [19]. They also secrete cAMP, a putative  
19 chemoeffector, during biofilm formation [20].

20 The behavior of zoospores in response to changes in ionic conditions suggests that cationic  
21 fluxes may be involved in collective motion, but their nature and precise role remain unclear.  $\text{Ca}^{++}$   
22 plays a key role in autonomous encystment, adhesion, germination and auto-aggregation [10],

1 but does not directly trigger cooperative behavior between zoospores, instead acting more like a  
2 secondary messenger [19, 21].  $K^+$  homeostasis influences the locomotion and encystment of  
3 zoospores. High external concentrations (5-10 mM) of potassium salts reduce the swimming  
4 speed of *P. palmivora* zoospores and cause them to swim in a jerky fashion [3]. Potassium sensing  
5 also triggers negative chemotaxis in the zoospores of *Phytophthora palmivora* [4].

6 We sought to characterize the signals altering the pattern of zoospore motility and  
7 initiating auto-aggregation or biofilm formation. Our findings suggest that the aggregation of *P.*  
8 *parasitica* zoospores is elicited by the perception of monocationic gradients in a particular  
9 geometric arrangement. Using macro- and microfluidic systems together with time-lapse live-cell  
10 imaging to measure the fluorescence intensity of impermeant cation probes, we defined the  
11 characteristics of the  $K^+$  gradients and zoospore motion.

12

## 1            **2. Materials and methods**

### 2            **2.1 Preparation of the zoospore suspension**

3            *P. parasitica* (isolate 310, *Phytophthora* INRA collection, Sophia- Antipolis) mycelium was  
4 routinely cultured on malt agar at 24°C in the dark. For zoospore production, mycelium was grown  
5 for one week in V8 liquid medium at 24°C, under continuous light. The material was then drained,  
6 macerated and incubated for a further four days on water agar (2%). The zoospores were released  
7 by heat shock treatment: incubation for 30 min at 4°C and then 20 minutes at 37°C. We added 10  
8 mL (per Petri dish  $\Phi$ 100 mm) of 2 mM Mes [2-(N-morpholino) ethanesulfonic acid]-NaOH buffer  
9 pH 6.5 between incubations. Zoospore concentration was adjusted to  $5 \times 10^5$  cells/mL.

### 10           **2.2. Droplet assay**

11           Three chemotaxis set-ups were used for zoospore motion studies. The first was a droplet  
12 assay (figure1). A controlled profile of the signal was generated by applying a [1 mM-1 M] gradient  
13 in a local oriented manner to a freshly prepared suspension of zoospores so as to achieve an  
14 essentially stable profile by diffusion. The basic operation involved the microinjection of putative  
15 chemoeffectors (1/200, V/V) at the periphery of droplets (200-500  $\mu$ L) including zoospores  
16 deposited on glass sides or PDMS (polydimethylsiloxane) stamps. Various conditions (in terms of  
17 ionic composition and strength, pH, nutrient supply and cell density) were tested, and K<sup>+</sup> sensing  
18 was identified as a primary signal for zoospore aggregation.

19

20

### 1           **2.3.    Passive dispersion system for the generation of ionic gradients**

2           A passive dispersion system was used to generate a diffusion gradient for the  
3 simultaneous measurement of extracellular potassium concentration on one hand and tracking  
4 of zoospores distribution on the other hand. Cells were preloaded with 2  $\mu$ M Asante Potassium  
5 Green-2 (APG-2 TMA<sup>+</sup> salt, Teflabs, 3622), a potassium-specific non-permeant fluorescent dye.  
6 We placed 50  $\mu$ L of cell suspension in a microchamber ( $\mu$ -Slide VI – Flat, Ibidi size l:17 mm; w: 3.8  
7 mm; h: 400  $\mu$ m), to which we added 0.5  $\mu$ L of 500 mM KCl. At various time points, the content of  
8 each chamber was observed with a confocal microscope (LSM 880-Zeiss) and the Tile Scan tool.  
9 Images (1.2 mm x 1.2 mm) were generated from the point of application and along the length of  
10 the chamber. APG-2 was excited with a 488 nm argon laser and the fluorescence emitted was  
11 captured in channel mode (band pass 510-590 nm). The distance between the point of application  
12 and the highest position in the chamber allowing zoospore motion was determined with a  
13 transmission-photomultiplier. The 1.2 mm x 0.4 mm area corresponding to this position was  
14 divided into three technical replicates (0.4 x 0.4) for the measurement of mean APG-2  
15 fluorescence intensity (FI) in each area. The highest ionic concentration allowing zoospore motion  
16 was calculated from the difference between the APG-2 FI measured at this position, before and  
17 after the addition of potassium, and relative to the FI values obtained with a range of discrete  
18 concentrations. Image analysis was performed with ZEN 2 software (Zeiss).

### 19           **2.4.    Microfluidic device**

20           The third set-up used to capture the immediate response of zoospores at the single-cell  
21 level consisted of a PDMS microfluidic circuit in which the zoospores were subjected to a

1 continuous flow presenting a gradient of potassium concentration. The main advantage of this  
2 approach is that it allows rapid and effective control over the conditions around the spores in the  
3 chamber.

4 This system is presented in figure 5A. Three channels ( $H \times W = 0.05 \text{ mm} \times 0.1 \text{ mm}$ )  
5 intersect as a cross, fusing into the final channel, which is much wider ( $H \times W = 0.2 \text{ mm} \times 1 \text{ mm}$ ).  
6 The spores are observed in this chemotactic chamber. Spores are injected into the middle inlet  
7 and the 100 mM KCl solution is injected into the two lateral channels. This device was produced  
8 by soft lithography techniques [22], with all the steps performed in the clean room of the Institut  
9 de Physique de Nice. SU-8 molds exposed at a resolution of 50800 DPI were covered with 10:1  
10 Sylgard PDMS for curation. They were unmolded and punctured for inlets and plasma bonding on  
11 clean glass slides was then used to seal the channels. Teflon tubing was directly inserted into the  
12 PDMS holes to connect the solution reservoirs (2 ml) to the system. Liquid flows were driven with  
13 a pressure controller (Fluigent), in the 0-100 mbar range between the three inlets and the outlet,  
14 which was at atmospheric pressure. A high-speed camera (Phantom v7.11) placed on a Zeiss  
15 Axiovert 200M inverted microscope with a x10 objective was used to film movies at a speed of  
16 200 fps.

### 17 **Microscopy for image acquisition along horizontal or vertical axes**

18 Zoospore motion was captured with several different instruments: a VHX-2000 digital  
19 microscope (Keyence); an LSM 880 inverted confocal microscope (Zeiss); an axioImagerZ1 (Zeiss)  
20 equipped for bright-field and epifluorescence microscopy; an Axioskop (Zeiss) microscope  
21 mounted vertically but rotated by  $90^\circ$  with appropriate support on the back of its frame for

1 imaging over a vertical plane. Movie acquisition was controlled by 3D profile VHX-H3M (Keyence)  
2 or ZEN (Zeiss) software, generating sequences of 10 to 30 seconds at 10-30 frames per second.

### 3 **2.5. Image analysis**

4 The dynamics of zoospore motion were first investigated by single-particle tracking with  
5 various image-processing algorithms available as plugins from the ImageJ or Fiji software libraries.  
6 The initial processing of phase-contrast zoospore images involved TIFF format conversion, image  
7 inversion, threshold adjustment and binary conversion. Velocity\_Measurement\_Tool plugins  
8 were used to generate kymographs. We used MosaicSuite [23] to draw trajectories. The  
9 TrackMate plugin [24] was used to track the zoospores in droplets. Movies were analyzed with  
10 the following parameters: estimated blob diameter, 16  $\mu\text{m}$  and threshold, 12  $\mu\text{m}$ ; automatic  
11 initial thresholding; linking max distance, 50  $\mu\text{m}$ ; gap-closing max distance, 50  $\mu\text{m}$ ; gap-closing  
12 max frame, 2; spot filtering: quality above 168; track filtering process: duration of track above 1.5  
13 s. For each remaining trajectory, we calculated instantaneous velocities between two successive  
14 points, which made it possible to calculate the mean velocity  $v_i$  for each trajectory  $i$ ; we  
15 calculated the mean velocity of the zoospores for a given movie as the mean  $v_i$ , together with the  
16 associated standard deviation.

17 We obtained velocity fields with the PIV (Particle Image Velocimetry) plugin applied to two  
18 sequential images (image size 1388 x 1040 pixels; time scale 1 s). Magnitude vector maps were  
19 generated with multiple-iteration window sizes of 128 x 128, 64 x 64 and 32 x 32 pixels.

### 1           **3. Results**

#### 2           **3.1. Potassium induces zoospore aggregation in a concentration-specific manner**

3           The droplet assay (figure 1) was used to evaluate specificity and to determine the optimal  
4 conditions for the detection of ion gradients by zoospores. Upright microscopes were used for  
5 observation in the horizontal plane (figure 1A). A microscope setup was adjusted so as to position  
6 the axis of the lens horizontally for observations of displacement in the vertical plane (figure 1B).  
7 Three states were defined and reproducibly observed (figure 2A): (i) a free state (FREE)  
8 corresponding to untreated cells, uniformly distributed throughout the droplet and displaying  
9 random motion; (ii) a swarm state (SWA), corresponding to ion-treated cells, with the upward  
10 migration of zoospores to form a swarm of increasing cell density in a progressively restricted  
11 area within minutes; (iii) an aggregate state (AGG) in which the zoospores formed a plume and  
12 migrated downward to collect together on the support surface.

13           The aggregation process occurred with potassium, regardless of the associated anion ( $\text{Cl}^-$ ,  
14  $\text{CH}_3\text{COO}^-$ ,  $\text{MnO}_4^-$ ,  $\text{SO}_4^{2-}$ ), over a pH range extending from 5 to 8, at a cell density of  $10^5$  to  $4 \times 10^6$   
15 zoospores/mL, and a quorum of  $5 \times 10^3$  to  $2 \times 10^4$  cells. Aggregation peaked within 12 to 15  
16 minutes when 0.5 to 3  $\mu\text{moles}$  of potassium was applied per 100  $\mu\text{l}$  of cell suspension at the  
17 starting point (Movie S1, figure 2A-D). We tested several other cations (Table 1).  $\text{Na}^+$  application  
18 also induced aggregation, but larger amounts of this cation than of  $\text{K}^+$  were required.  $\text{H}^+$  also  
19 affected the swimming behavior of zoospores but did not provoke aggregation, instead triggering  
20 a transient local gathering of zoospores (0.001 to 0.01  $\mu\text{moles}$ ) or ring formation followed by high  
21 rates of cell death for larger amounts. For subsequent analyses, the assays were performed at pH

1 6.5, with the application of 0.5  $\mu\text{mole}$  KCl per 100  $\mu\text{l}$  of a suspension of  $5 \times 10^5$  cells/mL. The  
2 objectives of this study were to explore the effects of  $\text{K}^+$  ions, which induce various behaviors of  
3 interest in the particular case of *Phytophthora*, and, more generally, to develop a model for the  
4 biophysics of swimming for a large number of swimming cells based on these effects.  $\text{K}^+$  has strong  
5 effects at low concentration (such as those found in natural environments), with weaker osmotic  
6 effects than  $\text{Na}^+$  ions, which would need to be used at concentrations 10 times higher. We  
7 therefore performed droplet assay experiments on various ions, but we focused exclusively on  
8 the effects of  $\text{K}^+$  ions in the milli- and micro-fluidic experiments.

9

### 10 **3.2. Behavior of zoospores sensing potassium**

11 In each state, we analyzed the distribution and displacement of zoospores in both the  
12 horizontal (figure 2E-J) and vertical (figure 2K-M) planes. In the FREE state, the projected  
13 velocities were  $150 \pm 34 \mu\text{m/s}$  in the horizontal plane, and  $146 \pm 39 \mu\text{m/s}$  in the vertical plane,  
14 and no preferential direction of cell trajectories was noted (figure 2B, E,H).

15 In the SWA state (figure 2C,F,I,L), the projected velocity in the horizontal plane was  $115 \pm$   
16  $29 \mu\text{m/s}$ , decreasing at the periphery of the swarm, as illustrated on the kymograph by the weak  
17 slope of the lines at the edge of the swarm for this plane (figure 2I). There was no clear  
18 preferential direction for trajectories in the horizontal plane, but all trajectories were delineated  
19 within the swarm (figure 2C, F). The velocity in the vertical plane was  $78 \pm 32 \mu\text{m/s}$ , and swarm  
20 formation in this plane was correlated with a continuous upward migration (Movie S2)

1 culminating in the accumulation of almost all cells at the air-liquid interface, with only a very small  
2 number of cells in the scanned area below (figure 2L). No such spectacular upward migration was  
3 observed for zoospores swimming freely in water (Movie S3, figure 2K).

4 In the AGG state and the horizontal plane (figure 2D, G, J), all zoospores migrated with  
5 centripetal trajectories (figure 2G), at very low velocity ( $V_{xy} = 24 \pm 11 \mu\text{m/s}$ ), toward a restricted  
6 area ( $1 \text{ to } 5 \times 10^6 \mu\text{m}^2$ ) in which they ceased moving linearly and formed an aggregate (Movie S1,  
7 figure 2D). The velocity in the vertical plane was  $41 \pm 19 \mu\text{m/s}$  (Movie S4, figure 2M). Once the  
8 plume had been formed, the cells abruptly began to migrate downward (plume velocity =  $65 \pm 23$   
9  $\mu\text{m/s}$ ; Movies S4 and S5). At the end of the sequence, the zoospores were alive and motile (Movie  
10 S6), and they bore flagella (figure S1), subsequently undergoing massive progressive encystment.  
11 Based on the number of zoospores sedimenting on the lower surface at the end of the experiment  
12 and the size of the plumes observed on microscopy, the density of zoospores in a plume has been  
13 estimated at about  $40 \times 10^3$  spores/ $\mu\text{L}$ .

14 Obviously, plume displacement included a large vertical component during downward  
15 migration (Movie S5; figure S2). This downward migration initially involved an almost rectilinear  
16 and vertical displacement for about 10s at a  $V_z$  of about  $50 \mu\text{m/s}$ . The trajectory then became  
17 helical, with a large decrease in  $V_z$ , probably when the cells reached the threshold  $\text{K}^+$   
18 concentration range defined below (figure S2C,D).

19 In this assay, we also analysed the effect of zoospore motion on fluid velocity, by adding  
20 fluorescent microspheres to the cell suspension. By tracking the movements of zoospores and  
21 microspheres simultaneously, we showed that fluid velocity was unaffected by zoospores

1 swimming freely or in a swarm at the time and spatial scales studied (data not shown). By  
2 contrast, during aggregation, zoospores migrating downward from the surface of the fluid caused  
3 microsphere advection (Movie S7). This finding was confirmed by PIV analysis, providing a picture  
4 of the local streamlines of the fluid velocity fields, which closely resembled the geometry,  
5 orientation, and magnitude of zoospore movement (figure 3A, B). Further confirmation was  
6 provided by the variation of local velocities calculated from zoospores and microspheres located  
7 within and outside the plume (figure 3C). Taken together, these data indicate that the downward  
8 migration of zoospores correlates with fluid advection. At the beginning migrations causes fluid  
9 advection, but then these phenomena are linked and can be mutually supportive.

### 10 **3.3 The distribution of potassium-sensing zoospores depends on the ionic gradient**

11 The concentration gradient was heterogeneous and difficult to control in the droplet  
12 assay. This assay was not, therefore, suitable for analyses of the relationship between zoospore  
13 distribution and the extracellular  $K^+$  concentration gradient. We investigated the behavior of  
14 zoospores in response to various concentrations of potassium, by generating a diffusion gradient  
15 in a millifluidic device (figure 4A). This device consisted basically of a single channel, with one inlet  
16 and one outlet. The cells were loaded into the channel ( $H \times W \times L = 400 \mu\text{m} \times 3.8 \text{ mm} \times 1.7 \text{ mm}$ )  
17 in the presence of APG-2, a  $K^+$ -sensing probe, before a spot application of KCl at the inlet. We  
18 followed the fluorescence dynamics of APG-2 upon ion binding and the change in zoospore  
19 distribution along the channel by confocal microscopy (figure 4A). Fluorescence intensity was  
20 measured to determine  $K^+$  concentration, which is plotted in figure 4B. The fluorescence intensity  
21 profile obtained indicated that the dynamic range of  $K^+$  concentration that could be resolved in

1 this device was [0-17 mM]. A small minority of the zoospores in the population could not swim,  
2 and these zoospores were mostly located in the immediate vicinity of the application spot. Most  
3 of the zoospores displayed no change in motion (velocity and random trajectory, data not shown),  
4 but their distribution was restricted. The cells displayed negative chemotaxis [4], with optimal  
5 conditions for swimming occurring away from the higher concentrations of potassium ions. The  
6 “no-swimming zone” expanded over time as the ions diffused away from the point of application.  
7 We used the measurements of APG-2 fluorescence intensity obtained to determine the range of  
8 higher concentrations compatible with zoospore motion at various time points (figure 4A and C).  
9 The cell distribution depended on local  $K^+$  concentration. The difference in this concentration  
10 between the two sides of the border between the swimming and no-swimming zones lay in a  
11 narrow range (1–4-mM). This range did not change significantly over time. In the chemotaxis  
12 assay, we monitored the zoospores for a period of 30 minutes. We observed no change in the  
13 characteristics of zoospore motion in the swimming zone, except that the zoospores were unable  
14 to move into the areas of high potassium concentration. Thus,  $K^+$ -mediated negative chemotaxis  
15 seems to have been initiated in these conditions, but was not sufficient to induce aggregation.

### 16 **3.4. Changes in zoospore motion in response to $K^+$ in a microfluidic device**

17 For the quantification of zoospore distribution and velocity following the application of a  
18  $K^+$  gradient, zoospores were subjected to different gradients of KCl in a microfluidic system (see  
19 methods). Zoospores were injected from the central inlet into a chemotaxis observation chamber,  
20 and the two side channels were perfused with KCl (figure 5A). Zoospores and KCl were first  
21 injected together, at  $t=0$ ; the flow of KCl was stopped for time T (ranging from 5 s to 15 s) to

1 achieve a partial flushing out of the KCl; the flow of zoospores was then also stopped, and  
2 zoospore movement was observed for at least 20s. A picture of the chamber is shown in figure  
3 5B (upper image).

4 In another experiment in the same set-up but without zoospores, the steps described  
5 above were performed with KCl mixed with the potassium probe APG-2, to obtain a  
6 spatiotemporal map of potassium concentration in the chamber. Due to the geometry of the  
7 microfluidic set-up, the KCl was concentrated towards the top and bottom (on the image) of the  
8 chamber, as shown in the snapshot presented in figure 5B (lower image).

9 We characterized the migration process, by tracking cells from  $t=T$  to  $t=T+20s$ , to extract  
10 their trajectories, calculate the local density of cells, and measure the velocity of individual cells.  
11 The area used for this analysis was restricted to the red window shown in figure 5B. The same  
12 area was used for the calculation of spatiotemporal potassium concentrations. Both spore density  
13 and potassium concentration were determined by the sliding window method (see §2.4.), by  
14 calculating the mean values in rectangular windows sliding along the direction of the potassium  
15 gradient (the  $y$  coordinate in our set-up).

16 The results are shown in figure 6. After KCl was flushed out for 5s, the vast majority of  
17 zoospores rapidly adopted circular trajectories (figure 6A and Movie S8), moving at low speed,  
18 below  $40 \mu\text{m/s}$  (figure 6D and 6G). The residual concentration of potassium was therefore  
19 assumed to be higher than the threshold of 3-5 mM, resulting in the immediate “freezing” of cell  
20 motion. The concentration profiles in figure 6D and 6G are consistent with this interpretation:

1 after 4s, potassium concentration exceeded 5 mM over more than half the observed area, and,  
2 after 16s, potassium concentration exceeded 10 mM over the entire area.

3 After KCl was flushed out for  $T=10$  s, some zoospores initially moved toward the central  
4 zone (figure 6B and Movie S9), as expected, to escape the high concentrations of potassium  
5 towards the top and bottom of the device. These zoospores followed linear trajectories and  
6 moved at relatively high speeds (above  $100 \mu\text{m/s}$ ) after 4s (figure 6E). Nevertheless, some cells  
7 initially present in the zones at the top and bottom of the device immediately adopted low-speed  
8 circular trajectories (figure 6B and 6E), suggesting that the concentration of potassium in these  
9 zones was too high for the cells to escape. After about 10 seconds, all the cells shifted to low-  
10 speed circular trajectories (not shown), suggesting that the potassium had diffused into the  
11 central zone and had reached the threshold concentration there too. Unfortunately, we were  
12 unable to measure the potassium concentration during this cycle. After 16 s, cells were traveling  
13 at speeds of less than  $40 \mu\text{m/s}$  in the central zone (figure 6H), consistent with a shift to low-speed  
14 circular trajectories.

15 Flushing out KCl for  $T=15$  s resulted in behavior similar to that observed for  $T=10$  s, except  
16 that the area in which the zoospores moved along linear trajectories at high speed was larger  
17 (Movie S10, figure 6C and 6F), and, after 16 s, the cells continued to move along linear trajectories  
18 at high speed (figure 6I). This suggests that the concentration of potassium was sufficiently low  
19 to allow the cells to move. The concentration profiles obtained after 4 s and 16 s (figure 6G and  
20 6I) are consistent with this interpretation, as the concentration of potassium ions remained below  
21 3 mM. Interestingly, we found that: (i) between 4 s and 16 s, the cells tended to migrate toward

1 the central zone, despite the very low concentration of potassium; (ii) after 16 s, zoospore density  
2 peaked whereas the concentration profile appeared to be flat. These observations suggest that  
3 motion leading to aggregation can be triggered by a cue other than potassium concentration.  
4 Further investigations are required to shed light on this behavior. In the last 12 s, the density of  
5 zoospores swimming in a central area of the chamber (a 400  $\mu\text{m}$  X 100  $\mu\text{m}$  window) was estimated  
6 at  $20 \times 10^3$  (SD= $1.10^3$ ) zoospores/ $\mu\text{L}$ .

## 1           **4. Discussion**

2           *Phytophthora* auto-aggregation has been associated with bioconvection patterns [15] or  
3 a combination of bioconvection and positive chemotaxis [11]. Potassium sensory cues regulates  
4 the behavior of *Phytophthora* potassium zoospores [3, 4]. In this report, we present *in vitro*  
5 evidence that potassium gradient sensing by *P. parasitica* zoospores is a primary stimulus,  
6 inducing synchronized zoospore behavior and cell aggregation. The resulting macroscopic pattern  
7 resembles auto-aggregation. Cell behavior changes during a single biphasic temporal sequence  
8 different from that previously described for auto-aggregation.

### 9           **4.1. Negative chemotaxis and bioconvection**

10           Negative chemotaxis in response to the sensing of potassium initially causes the cells to  
11 move into a region in which potassium concentration is below the threshold range of 1-4 mM.  
12 The arrangement of the cells results in their spatial concentration. Within a droplet, negative  
13 chemotaxis increases cell concentration through upward migration toward the upper surface of  
14 the suspensions. The simultaneous accumulation of cells in the horizontal plane suggests that  
15 positive chemotaxis may also occur. Upward migration increases local mass density in the  
16 uppermost regions of the suspension, which become denser than the regions below them. This  
17 leads to the development of overturning instability, analogous to bioconvection, resulting in the  
18 formation of descending plumes of dense cell suspension, with fluid flow advection in their wake.  
19 We can compare the measured frontal velocity (section 3.2;  $65 \pm 23 \mu\text{m/s}$ ) with a simple model,  
20 by assuming that the plume is a single sedimenting object. We can start by comparing an  
21 individual sedimenting spore and then move up to the level of a whole plume, assimilated to a

1 drop of a heavier liquid falling into water. The sedimentation speed of a passive zoospore is about  
 2  $V_{ss}=2*Rs^2*g*\Delta\rho/(9\mu)$ , where  $Rs$  is the average radius of the spore (3.2  $\mu\text{m}$ ),  $g=9.81\text{m/s}^2$ , and  
 3  $\mu=0.001$ , the viscosity of water.  $\Delta\rho$  is assumed to be  $80\text{ kg/m}^3$ , corresponding to a spore density  
 4 of 1.08, a typical value for yeast cells or bacteria. We obtained a value of  $1.79\text{ }\mu\text{m/s}$  for  $V_{ss}$ . For  
 5 plume speed,  $V_{sp}$ , we used the same formula as for a spherical object falling, but using  $R=450$   
 6 microns rather than  $Rs$ , the mass density being the mean density of the water/spore suspension  
 7 (For  $N=4000$  spores in the plume):  $\Delta\rho_p=\Delta\rho*N*Rs^3/R^3=0.12\text{ kg/m}^3$ .  $V_{sp}=2*R^2*g*\Delta\rho_p/(9\mu) =$   
 8  $V_{ss}*N*Rs/R$ , and with  $Rs/R = 0.007$ , we obtain  $V_{sp}=51\text{ }\mu\text{m/s}$ . This provides us with an approximate  
 9 order of magnitude close to the measured values, given that  $N$  is not precisely determined and  
 10 the exact flow conditions between spores are not exactly known.

11 Based on the congruent results of the droplet (in the vertical and horizontal planes) and  
 12 microfluidic (horizontal plane) assays, we can suggest the following scheme. If  $\text{K}^+$ -treated cells are  
 13 able to escape from high concentration areas, they follow a linear trajectory and head toward  
 14 areas in which the potassium concentration is below the threshold of 1-4mM. When conditions  
 15 restrict the cells to areas in which the potassium concentration is beyond this threshold, two  
 16 drastic changes are observed: velocity decreases sharply and the cells switch from a linear  
 17 trajectory to a helical one. The  $\text{K}^+$ -induced aggregation phenomenon was observed when the  
 18 motion of a quorum of zoospores ( $5 \times 10^3$ -  $2 \times 10^4$ ) explored territories delimited by the  
 19 concentration field and its spatial distribution in the various set-ups used here. In both the droplet  
 20 assay and the microfluidic device, the maximum density of zoospores was estimated at a few tens  
 21 of thousands of zoospores per microliter. This may constitute a threshold value for the density of  
 22 *P. parasitica* zoospores. However, zoospores seemed to be able to remain clustered for longer at

1 higher spatiotemporal variations of the  $K^+$  gradient in microfluidic devices, suggesting that  
2 signaling between zoospores may result in a stronger response.

3

#### 4 **4.2. Sources of $K^+$ gradients in the natural environment**

5 The induction of zoospore clustering by  $K^+$  *in vitro* demonstrates that aggregation may  
6 result from the perception of an external signals. How can such gradients be achieved in natural  
7 habitats? Such efflux mechanisms could be generated by efflux from zoospores released from  
8 other microbes present in the same biotope, rhizospheric activity and/or exchange dynamics in  
9 soil.

10 The self-generation of  $K^+$  by a net  $K^+$  zoospore efflux seems highly unlikely. In freshwater,  
11 the osmolality of the zoospore cytosol is always higher than that of the external environment.  
12 Throughout the course of their displacement, one of the major challenges faced by wall-less  
13 zoospores is the removal of excess cytosolic water rather than ions to maintain homeostasis. The  
14 excess water collects in the contractile vacuole complex (CVC), the osmoregulatory organelle, and  
15 is discharged into the extracellular environment [7]. A calculation of the  $K^+$  diffusion potential of  
16 cells also rules out the hypothesis of  $K^+$  efflux from zoospores. If we consider high densities ( $10^6$ -  
17  $10^7$ /mL) of zoospores (diameter of 10  $\mu\text{m}$ ), and an intracellular  $K^+$  concentration range of 100-200  
18 mM, then the relative volume expansion rate of the cell population ranges from 0.052 to 0.52%.  
19 This would result in an extracellular  $K^+$  concentration of between 0.05 and 1 mM if the entire  
20 potassium content of the cell were released by efflux. It would not, therefore, be possible to reach  
21 the threshold concentration of 1-4 mM identified here as the stimulus eliciting a pattern

1 reminiscent of autoaggregation. Instead, as in most prokaryotic and eukaryotic cells [25],  
2 depolarization due to the increase in extracellular potassium concentration may lead to  
3 fluctuations of the membrane potential of zoospores, potentially modifying the beating of the  
4 flagella, cellular responses, such as osmoregulation, and/or cell-to-cell signaling.

5         The extent to which  $K^+$  release from the microbiota present in the same habitat as the  
6 zoospores can mediate zoospore aggregation remains to be evaluated. Potassium seems to play  
7 a key role in the displacement of bacteria, the physical composition of microbiota [25] and  
8 pathogenic processes [26]. The electrical signaling mediated by potassium ion channels regulates  
9 cell-cell dialog within bacterial biofilms, with potassium driving the attraction of distant cells of  
10 different species [25]. The range of bacterially generated gradients effective for prokaryote  
11 attraction *in vitro*, is of the same order of magnitude as that affecting zoospore movement in our  
12 experiments. Such gradients may, therefore, affect the distribution of *P. parasitica* propagules  
13 through repulsion.

14         In terms of rhizosphere activity and exchange dynamics in the soil, any area in which  
15 strong  $K^+$  gradients are generated will tend to repel *P. parasitica* zoospores. The total  $K^+$  content  
16 of soils generally ranges between 0.4 and 30 g  $kg^{-1}$  [27], and has two components. Soil particles,  
17 which bind about 98% of the total  $K^+$  content, may constitute a major obstacle to zoospore  
18 tracking. The film of water surrounding these particles (2% of total  $K^+$  content) has a potassium  
19 concentration in the range of 0.2-15mM, reaching 5-10 mM in the most highly fertigated  
20 agricultural soils [27]. It is therefore reasonable to speculate that  $K^+$  exchange dynamics in the soil  
21 constitute a major parameter determining zoospore distribution and aggregation. At the scale of  
22 an infected host plant, zoospores repelled by soil particles and subject to constraints on their

1 movement in the water film would be likely to move toward host tissues. This tendency would be  
2 enhanced by root  $K^+$  uptake, which would result in a zone of potassium depletion around the root  
3 surface [28], and by root exudates, which attract zoospores [1, 29]. Thus, the physical and  
4 chemical distribution of  $K^+$  at the soil-root interface is a parameter that may contribute to the  
5 constitution of a high-density inoculum or biofilm formation on the plant surface. However, the  
6 importance of this contribution relative to other ion exchange dynamics, such as soil acidification  
7 by roots, remains to be determined. A more holistic view of the relationships between the  
8 concentrations of various ions and zoospore distribution is required to determine the influence  
9 of  $K^+$ .

10

### 11 **4.3. Concluding remarks**

12 We show here that the sensing of a potassium gradient induces synchronized zoospore  
13 behavior (due to negative chemotaxis) and the aggregation of *P. parasitica* zoospores. In all the  
14 *in vitro* experimental set-ups used (droplet assays, milli- and micro- fluidic devices), the zoospores  
15 displayed the same behavior, with a clear, consistent response to potassium. The use of these  
16 different set-ups shed light on particular aspects linked to the size and geometric effects of each  
17 of the set-ups used. Bioconvection patterns followed by aggregation were observed only in  
18 droplet assays. Nevertheless, in millifluidic devices, clear and quantitative response to potassium  
19 gradients were demonstrated, and the zoospores aggregated, reaching a density of the same  
20 order of magnitude as that observed in droplets. The microfluidic devices allowed faster  
21 spatiotemporal variations of potassium concentration, making it possible to observe the

1 clustering process, which appeared to be stronger than the response expected on the basis of  
2 quasi-static negative chemotaxis. Thus, even when the potassium concentration fell to low values  
3 compatible with zoospore movement, the zoospores remained clustered, at least transiently.  
4 Future studies should try to identify the signals released by zoospores in the presence of  $K^+$   
5 responsible for promoting autoaggregation behavior. More complex microfluidics devices and a  
6 modeling approach are being developed with this aim in mind, for future studies.

7

1 **Table 1— Effect of the anisotropic application of cations on zoospore pattern formation**

Effect of the anisotropic application of cations on zoospore pattern formation					
Cation	Amount μmoles	Swarm	Plume	Aggregate	Volume μL
K <sup>+</sup>	[0.5-3]	YES	YES	YES	100
Na <sup>+</sup>	[5-30]	YES	YES	YES	100
H <sup>+</sup>	[10 <sup>-3</sup> -10 <sup>-2</sup> ]	YES	NO	NO	100
Ca <sup>++</sup>	[0.5-3]	NO	NO	NO	100
Cu <sup>++</sup>	[0.5-3]	NO	NO	NO	100
Mg <sup>++</sup>	[0.5-3]	NO	NO	NO	100
Zn <sup>++</sup>	[0.5-3]	NO	NO	NO	100
NH <sub>4</sub> <sup>+</sup>	[0.5-3]	NO	NO	NO	100

The first and second rows indicate the identity and ranges of the amount of cation (chloride salt) added to a droplet (100 μl); YES/NO for the induction or non-induction of a swarm, plume or aggregate upon cation application

2

3

1  
2  
3  
4  
5  
6  
7  
8  
9  
10  
11  
12  
13  
14  
15  
16  
17  
18  
19  
20  
21

**Figure Legends**

**Figure 1: Schematic views of the droplet assay**

Potassium was applied at the base of each droplet containing zoospores and at a point on the circumference. Subsequent characterization of the metrics of zoospore motion was based on micrographs generated in either the horizontal (**A**) or vertical (**B**) plane.

**Figure 2: Zoospore motion in droplets in response to K<sup>+</sup> application**

**(A)** Summary scheme of the distribution and displacement of the cell population in three different defined states: **FREE** for zoospores swimming freely and distributed randomly before gradient sensing; **SWA** and **AGG** for zoospores forming a swarm and aggregating, respectively, upon gradient sensing. The range is indicative of the time at which each sequence occurred after KCl application. **(B)** to **(J)** illustrate patterns observed in the horizontal plane for zoospore distribution (**B, C, D**), swimming paths (**E, F, G**) and 2D-kymographs drawn for 10 s (**H, I, J**). The kymographs provide a picture of the variation of zoospore behavior in the 3 states, from highly motile cells, appearing as oblique lines (**H**), to more static cells represented by vertical lines (**J**). Swimming paths were recorded for x,y coordinates corresponding to the areas delimited by dotted rectangles in **B, C** and **D** for 2 s for (**E, F**) or 4 s for (**G**). The color coding provides information about mean velocity with range-limiting values indicated at the bottom of each inset in  $\mu\text{m/s}$ . On the kymograph image, the vertical axis represents time (white arrow), the horizontal axis corresponds to the intensity of the pixel along the length of the selected line: a line ROI of 1500

1  $\mu\text{m}$  located at the center of the field along the  $x$  axis. (**K**, **L**, **M**) illustrate the distribution and  
2 displacement patterns observed in the vertical plane. The upper insets show representative  
3 micrographs for the FREE, SWA and AGG states. For each state, the lower insets show plots of  
4 zoospore number per unit area versus time, at each depth identified by the color code defined in  
5 the upper insets. The SWA state is associated with an upward migration (signified by an ascending  
6 red arrow) whereas AGG is associated with a downward migration (descending red arrow). The  
7 bidirectional and sequential movement of the cell population results in a five to seven-fold  
8 increase in local cell density during downward migration (compare **K** to **M**). The zoospore numbers  
9 presented are means calculated from three consecutive unit areas and are based on counts of  
10 particles of 3 to 30  $\mu\text{m}$  in diameter on converted binary images. Bar sizes: 100  $\mu\text{m}$

11

### 12 **Figure 3: Flow field of the water and velocity field of zoospores within a plume**

13 The flow field was analyzed by adding fluorescent microspheres ( $\Phi$  0.5  $\mu\text{m}$ ; 1/1000, v/v) to the  
14 cell suspension. One representative instance of a zoospore swimming within a plume was  
15 visualized in the horizontal plane (Movie S7). The movement of zoospores was captured by dark-  
16 field microscopy during the first six seconds of the sequence. The movement of fluorescent  
17 microspheres was then captured for 5 s by switching to fluorescence microscopy with a rhodamine  
18 fluorescence filter set. (**A**) A vector magnitude plot of velocity fields, defined by the PIV of  
19 zoospore movement and generated between  $t=5$  s and  $t=6$  s. (**B**) The vector magnitude plot of  
20 the microsphere movement was generated between  $t=7$  s and  $t=8$  s, one second after the switch  
21 from dark-field to fluorescence microscopy. The color code indicates the magnitude of velocity

1 ( $\mu\text{m/s}$ ). **(C)** Histogram of the mean velocity of zoospores and microspheres determined from areas  
2 located outside (dotted yellow square in (A) and (B)) or within (dotted white squares in (A) and  
3 (B)) the plume. The difference between the values determined within and outside the plume were  
4 highly significant for both particles in Student's *t* test ( $P < 0.0001$ )

5  
6 **Figure 4: A potassium gradient drives zoospore distribution in a passive dispersion system**

7 **(A)** The millifluidic device ( $H \times W = 400 \mu\text{m} \times 3.8 \text{ mm}$ ) is shown at the top. The two images  
8 below show a characteristic APG-2 fluorescent signal pattern captured by confocal laser  
9 microscopy (upper left panel), and the corresponding area ( $12 \text{ mm}^2$ ) observed by transmission with  
10 a T-PMT detector (upright panel) in a millifluidic device. The blank point corresponds to the site  
11 of application of  $1 \mu\text{L}$  of  $0.5\text{M}$  KCl at  $t=0$  and the dotted line indicates the total distance screened  
12 ( $10 \text{ mm}$ ) at 1, 3, 5 and 10 min. The lower panel focuses on an area ( $0.48 \text{ mm}^2$ ) in which the fields  
13 of the device in which zoospore motion can and cannot be observed can be delimited. The  
14 location of encircled zoospores defines, at time  $t=5 \text{ min}$ , the transition between the two fields  
15 characterized by the presence/absence of cells. **(B)** Measurement of fluorescence intensity across  
16  $1,000 \mu\text{m}$  of the chamber, defining the concentration profile, which follows a non-linear gradient.  
17 **(C)** Box plot of the highest ion concentrations compatible with zoospore motion. Minimum and  
18 maximum values are depicted by white dots; the box indicates the upper and lower quartiles, the  
19 mean and the median are represented by + and a white rectangle within the box, respectively,  
20 for each raw datum. The values indicated are the means of 5, 6, 5 and 4 replicates for 1, 3, 5 and  
21 10 min, respectively.

1

2 **Figure 5: Microfluidic device**

3 (A) Image of the device, showing the three inlets and the chemotactic chamber (H x W =  
4 0.2 mm x 1 mm). Zoospores were injected into the central inlet and 100 mM KCl was injected into  
5 the side inlets (signal inlets). (B) Images of the observation chamber (or chemotactic chamber) in  
6 bright-field conditions (upper image), showing zoospores, and in fluorescence conditions (lower  
7 picture), for the mapping of potassium concentration in the chamber based on the fluorescence  
8 of the APG-2 probe. The red window indicates the area of the chamber taken into account in the  
9 analysis of zoospore tracking and measurement of the spatiotemporal concentration of  
10 potassium. In the lower images, the white areas in the uppermost and lowermost regions of  
11 image indicate the areas in which the concentration of potassium is high.

12

13

14 **Figure 6: Trajectories, density profiles and the speed of the zoospores in the chamber,**  
15 **according to potassium concentration profile**

16 Trajectories of the zoospores throughout the entire chamber after the flushing out of KCl  
17 for a time T equal to 5 s (A), 10 s (B) and 15 s (C, only one tenth of the trajectories are shown for  
18 the sake of simplicity). (D-E-F): Local density of zoospores (squares) with a color map for the

1 associated velocity, and the potassium profile (red lines), the flushing out of KCl for 4 s. (G-H-I):  
2 same representations after 16 s of KCl flushing.

3

#### 4 **Supplementary data legends**

#### 5 **Figure S1: Distribution of K<sup>+</sup>-treated and aggregated zoospores**

6 Before potassium treatment, the zoospores were stained with 0.001% Nile Red and mixed  
7 with 10 μm-diameter polystyrene microspheres. After treatment ( $t=20$  min), the distributions of  
8 the microspheres and zoospores were observed with a bright-field transmitted light detector (**A**).  
9 The zoospores stained with the fluorescent dye were observed with excitation at 514 nm and  
10 emission at 534 to 700 nm (**B**). The comparison between **A** and **B** illustrates the homogeneous  
11 distribution of the microspheres, whereas the aggregated zoospores were restricted to an area  
12 of  $1.8 \times 10^6 \mu\text{m}^2$ . (**C**) Micrograph showing biflagellate zoospores fixed in 1% paraformaldehyde  
13 immediately after aggregation and stained with 0.001% Nile Red. Bar sizes: 1000 μm in **A** and **B**;  
14 10 in μm **C**

#### 15 **Figure S2: Downward migration in droplets**

16 (**A**) Time series of selected views illustrating the vertical changes in plume sedimentation  
17 observed in a droplet assay. (**B**) Box plot of the sedimentation rate measured for plumes (at the  
18 sedimentation front) and floating isolated cells. (**C**) The images illustrate the change in zoospore  
19 trajectories over time during downward migration. The trajectories were plotted during six  
20 successive five-second sequences, as indicated in the square brackets. The color coding indicates

1 the mean velocity and the range-limiting values are indicated at the top of each inset ( $\mu\text{m/s}$ ). (**D**)  
2 Vertical velocity parameters for three representative zoospores. The left panels show trajectories  
3 tracked for least 15 s, with dotted lines delineating two patterns: a linear vertical pattern, and a  
4 helical pattern discernable at the lower end of trajectories. The upper right panel shows the  
5 vertical velocity kinetics. The lower panel shows a map of point density generated from the  $x/z$   
6 coordinates of each of the three trajectories with the Gaussian kernel density tool of PAST3 [30].  
7 Scaling provides an estimate of the number of points per unit area and illustrates the low point  
8 density during downward migration. Bar sizes: 100  $\mu\text{m}$ .

9

#### 10 **Movie S1**

11 Sequences of events leading to zoospore aggregation observed by dark-field microscopy  
12 and on an upright microscope (observation in the horizontal plane). The movie shows six  
13 sequences: (1) FREE state, (2) and (3) SWA state in the periphery of the swarm, (4) SWA state, (5)  
14 and (6) AGG state.

#### 15 **Movie S2**

16 Upward migration (SWA state) observed with a vertical mounted microscope (observation  
17 in the vertical plane) following the application of  $\text{K}^+$

#### 18 **Movie S3**

19 Motion of zoospores swimming freely (FREE state) before  $\text{K}^+$  application, captured in the  
20 vertical plane

1        **Movie S4**

2        Downward migration (AGG state) observed with a vertical mounted microscope  
3        (observation in the vertical plane) following the application of  $K^+$

4        **Movie S5**

5        Vertical displacement of plumes during downward migration (the width of the central  
6        plume is  $\sim 800 \mu\text{m}$ ).

7        **Movie S6**

8        Cell population observed 30 min post  $K^+$ -treatment on the bottom surface of the sample,  
9        with motionless cysts and zoospores moving mostly in an anticlockwise rotation.

10       **Movie S7**

11       Displacement of zoospores and fluorescent microspheres visualized in the horizontal plane  
12       during downward migration of the plume. The particles were successively captured in the  
13       same sequence: first by dark-field microscopy for zoospores (from 1 to 8 s) and then by  
14       fluorescence microscopy for microspheres (from 10 to 16 s).

15       **Movie S8**

16       In the microfluidic device, zoospore behavior in the chemotactic chamber following KCl  
17       flushing for 5 s

18       **Movie S9**

1 In the microfluidic device, zoospore behavior in the chemotactic chamber following KCl  
2 flushing for 10 s

3 **Movie S10**

4 In the microfluidic device, zoospore behavior in the chemotactic chamber following KCl  
5 flushing for 15 s

1  
2  
3  
4  
5  
6  
7  
8  
9  
10  
11  
12  
13  
14  
15  
16  
17  
18  
19  
20  
21  
22  
23  
24  
25  
26  
27  
28

### **Authors' contributions**

EG and XN designed the experiments.

EG and CE carried out droplet and millifluidic analyses.

XN, CC and PT carried out microfluidic analyses.

EG, XN, CC, PT wrote the manuscript.

### **Acknowledgments**

We thank the Microscopy Platform-Sophia Agrobiotech Institut- INRA 1355-UNS-CNRS 7254- INRA PACA Sophia Antipolis for providing us with access to instruments and technical advice. The authors would like to thank Fernando Peruani, Emiliano Perez Ipiña (LJAD, Nice) and Laurent Counillon (LP2M, Nice) for fruitful discussions.

### **Data accessibility**

Movies used in this work are available and uploaded as electronic supplementary material.

### **Funding**

This work was supported by the French government, through the UCAJEDI Investments in the Future project managed by the National Research Agency (ANR) under reference number ANR-15-IDEX-01; through the "Credits Scientifiques Incitatifs" of the University of Nice Sophia-Antipolis and the "Action Recherche" of the INRA Plant Health and Environment Division.

### **Competing interests**

The authors have no competing interests to declare.

1

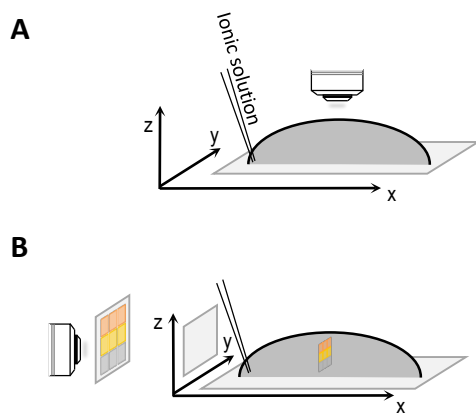
2 **References**

- 3 [1] Judelson, H.S. & Blanco, F.A. 2005 The spores of *Phytophthora*: weapons of the plant destroyer. *Nat*  
4 *Rev Microbiol* **3**, 47-58. (doi:10.1038/nrmicro1064).
- 5 [2] Walker, C.A. & van West, P. 2007 Zoospore development in the oomycetes. *Fungal Biology Reviews* **21**,  
6 10-18. (doi:<http://dx.doi.org/10.1016/j.fbr.2007.02.001>).
- 7 [3] Appiah, A.A., van West, P., Osborne, M.C. & Gow, N.A. 2005 Potassium homeostasis influences the  
8 locomotion and encystment of zoospores of plant pathogenic oomycetes. *Fungal Genet Biol* **42**, 213-223.  
9 (doi:10.1016/j.fgb.2004.11.003).
- 10 [4] Cameron, J.N. & Carlile, M.J. 1980 Negative chemotaxis of zoospores of the fungus *Phytophthora*  
11 *palmivora* *J Gen Microbiol* **120**, , 347-353.
- 12 [5] Morris, P.F. & Ward, E.W.B. 1992 Chemoattraction of zoospores of the soybean pathogen,  
13 *Phytophthora sojae*, by isoflavones. *Physiological and Molecular Plant Pathology* **40**, 17-22.  
14 (doi:[http://dx.doi.org/10.1016/0885-5765\(92\)90067-6](http://dx.doi.org/10.1016/0885-5765(92)90067-6)).
- 15 [6] van West, P., Morris, B.M., Reid, B., Appiah, A.A., Osborne, M.C., Campbell, T.A., Shepherd, S.J. & Gow,  
16 N.A.R. 2002 Oomycete plant pathogens use electric fields to target roots. *Molecular Plant-Microbe*  
17 *Interactions* **15**, 790-798. (doi:Doi 10.1094/Mpmi.2002.15.8.790).
- 18 [7] Hardham, A.R. 2007 Cell biology of plant-oomycete interactions. *Cell Microbiol* **9**, 31-39.  
19 (doi:10.1111/j.1462-5822.2006.00833.x).
- 20 [8] Kibdani, N., Pieuchot, L., Deleury, E., Panabieres, F., Le Berre, J.Y. & Gourgues, M. 2010 Cellular and  
21 molecular characterization of *Phytophthora parasitica* appressorium-mediated penetration. *New Phytol*  
22 **185**, 248-257. (doi:10.1111/j.1469-8137.2009.03048.x).

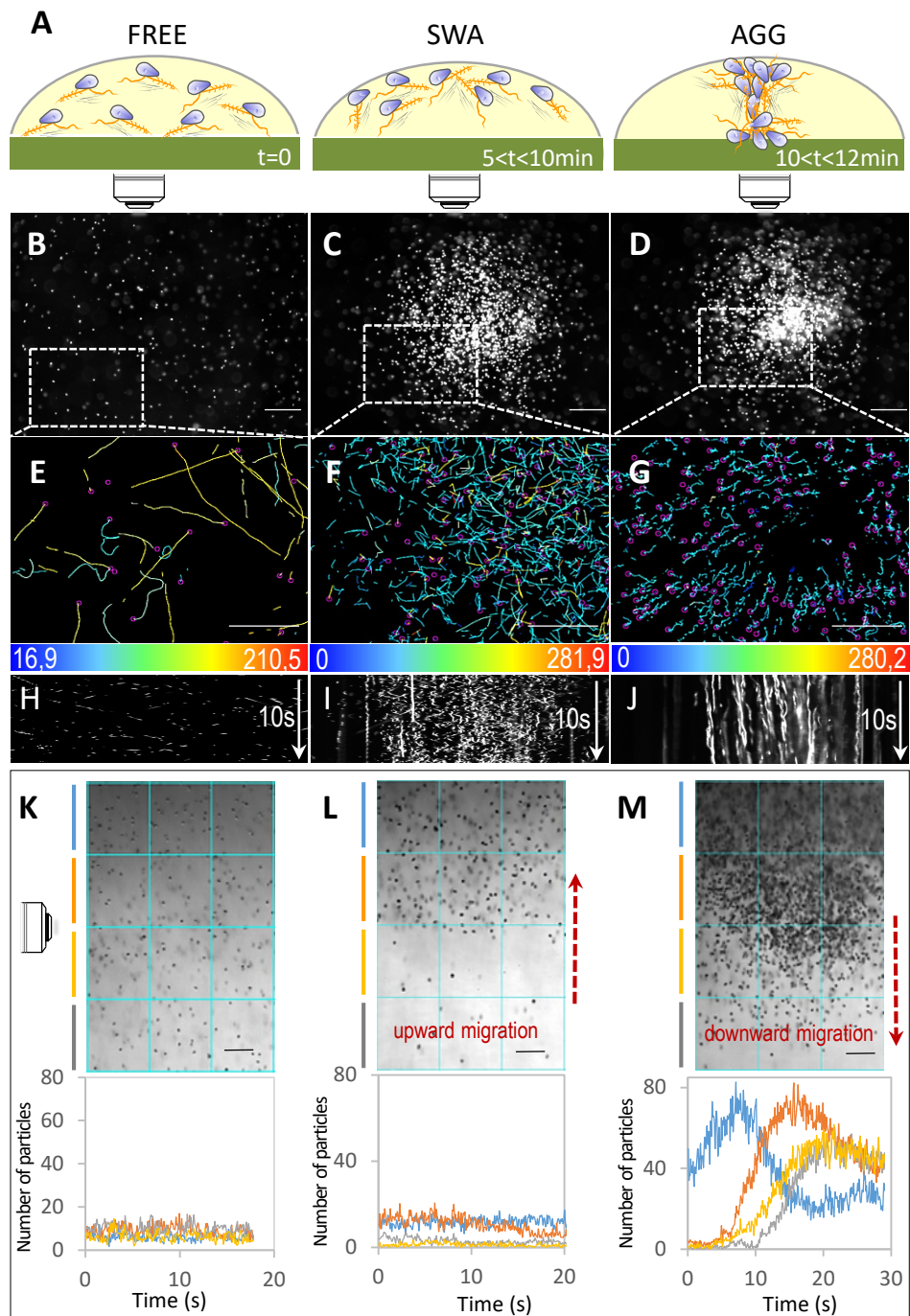
- 1 [9] Le Berre, J.Y., Engler, G. & Panabieres, F. 2008 Exploration of the late stages of the tomato-  
2 *Phytophthora parasitica* interactions through histological analysis and generation of expressed sequence  
3 tags. *New Phytol* **177**, 480-492. (doi:10.1111/j.1469-8137.2007.02269.x).
- 4 [10] Reid, B., Morris, B.M. & Gow, N.A.R. 1995 Calcium-dependent, genus-specific, autoaggregation of  
5 zoospores of phytopathogenic fungi. *Experimental Mycology* **19**, 202-213. (doi:DOI  
6 10.1006/emyc.1995.1025).
- 7 [11] Savory, A.I.M., Grenville-Briggs, L.J., Wawra, S., van West, P. & Davidson, F.A. 2014 Auto-aggregation  
8 in zoospores of *Phytophthora infestans*: the cooperative roles of bioconvection and chemotaxis. *Journal*  
9 *of the Royal Society Interface* **11**. (doi:ARTN 20140017  
10 10.1098/rsif.2014.0017).
- 11 [12] Larousse, M. & Galiana, E. 2017 Microbial partnerships of pathogenic oomycetes. *PLoS Pathog* **13**,  
12 e1006028. (doi:10.1371/journal.ppat.1006028).
- 13 [13] Larousse, M., Govetto, B., Seassau, A., Etienne, C., Industri, B., Theodorakopoulos, N., Deleury, E.,  
14 Ponchet, M., Panabieres, F. & Galiana, E. 2014 Characterization of PPMUCL1/2/3, three members of a new  
15 oomycete-specific mucin-like protein family residing in *Phytophthora parasitica* biofilm. *Protist* **165**, 275-  
16 292. (doi:10.1016/j.protis.2014.03.003).
- 17 [14] Kemen, E. 2014 Microbe-microbe interactions determine oomycete and fungal host colonization. *Curr*  
18 *Opin Plant Biol* **20**, 75-81. (doi:10.1016/j.pbi.2014.04.005).
- 19 [15] Ochiai, N., Dragiila, M.I. & Parke, J.L. 2011 Pattern swimming of *Phytophthora citricola* zoospores: an  
20 example of microbial bioconvection. *Fungal Biol* **115**, 228-235. (doi:10.1016/j.funbio.2010.12.006).
- 21 [16] Hill, N.A. & T.J., P. 2005 Bioconvection. *Fluid Dyn. Res.* **37**, 1–20. (doi:10.1016/j.fluiddyn.2005.03.002).
- 22 [17] Kessler, J.O. 1986 Individual and collective fluid dynamics of swimming cells. *J. Fluid Mech.* **173**.  
23 (doi:10.1017/S0022112086001131).

- 1 [18] Pedley, T.J. & Kessler, J.O. 1992 Hydrodynamic phenomena in suspensions of swimming micro-  
 2 organisms. *Annu. Rev. Fluid Mech.* **24**, 313–358. (doi:10.1146/annurev.fl.24.010192.001525).
- 3 [19] Kong, P. & Hong, C. 2010 Zoospore density-dependent behaviors of *Phytophthora nicotianae* are  
 4 autoregulated by extracellular products. *Phytopathology* **100**, 632-637. (doi:10.1094/PHYTO-100-7-0632).
- 5 [20] Galiana, E., Fourre, S. & Engler, G. 2008 *Phytophthora parasitica* biofilm formation: installation and  
 6 organization of microcolonies on the surface of a host plant. *Environ Microbiol* **10**, 2164-2171.
- 7 [21] Zheng, L. & Mackrill, J.J. 2016 Calcium signaling in oomycetes: an evolutionary perspective. *Front*  
 8 *Physiol* **7**, 123. (doi:10.3389/fphys.2016.00123).
- 9 [22] McDonald, J.C., Duffy, D.C., Anderson, J.R., Chiu, D.T., Wu, H., Schueller, O.J. & Whitesides, G.M. 2000  
 10 Fabrication of microfluidic systems in poly(dimethylsiloxane). *Electrophoresis* **21**, 27-40.  
 11 (doi:10.1002/(SICI)1522-2683(20000101)21:1<27::AID-ELPS27>3.0.CO;2-C).
- 12 [23] Sbalzarini, I.F. & Koumoutsakos, P. 2005 Feature point tracking and trajectory analysis for video  
 13 imaging in cell biology. *J Struct Biol* **151**, 182-195. (doi:10.1016/j.jsb.2005.06.002).
- 14 [24] Tinevez, J.Y., Perry, N., Schindelin, J., Hoopes, G.M., Reynolds, G.D., Laplantine, E., Bednarek, S.Y.,  
 15 Shorte, S.L. & Eliceiri, K.W. 2017 TrackMate: An open and extensible platform for single-particle tracking.  
 16 *Methods* **115**, 80-90. (doi:10.1016/j.ymeth.2016.09.016).
- 17 [25] Humphries, J., Xiong, L., Liu, J., Prindle, A., Yuan, F., Arjes, H.A., Tsimring, L. & Suel, G.M. 2017 Species-  
 18 independent attraction to biofilms through electrical signaling. *Cell* **168**, 200-209 e212.  
 19 (doi:10.1016/j.cell.2016.12.014).
- 20 [26] Yost, S., Duran-Pinedo, A.E., Krishnan, K. & Frias-Lopez, J. 2017 Potassium is a key signal in host-  
 21 microbiome dysbiosis in periodontitis. *PLoS Pathogens* **13**. (doi:ARTN e1006457  
 22 10.1371/journal.ppat.1006457).
- 23 [27] Sparks, D.L. 1987 Potassium dynamics in soils *Advances in Soil Science*. Springer, pp. 1-63. .

- 1 [28] Maathuis, F.J.M. & Sanders, D. 1996 Mechanisms of potassium absorption by higher plant roots.  
2 *Physiologia Plantarum* **96**, 158-168.
- 3 [29] Gow, N.A.R. 2004 New angles in mycology: studies in directional growth and directional motility (vol  
4 108, pg 5, 2004). *Mycological Research* **108**, 466-410. (doi:10.1017/S0953756204000097).
- 5 [30] Hammer, Ø., Harper, D.A.T. & Ryan, P.D. 2001 PAST: Paleontological statistics software package for  
6 education and data analysis. *Palaeontologia Electronica* **4**, 9pp.
- 7

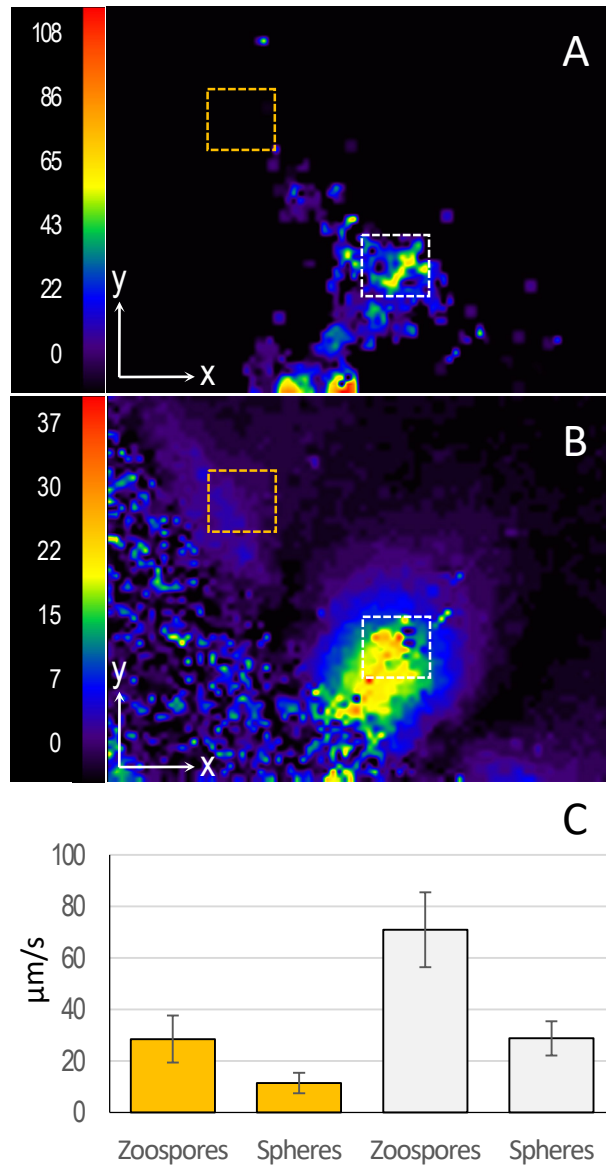


**FIGURE 1**

**FIGURE 2**

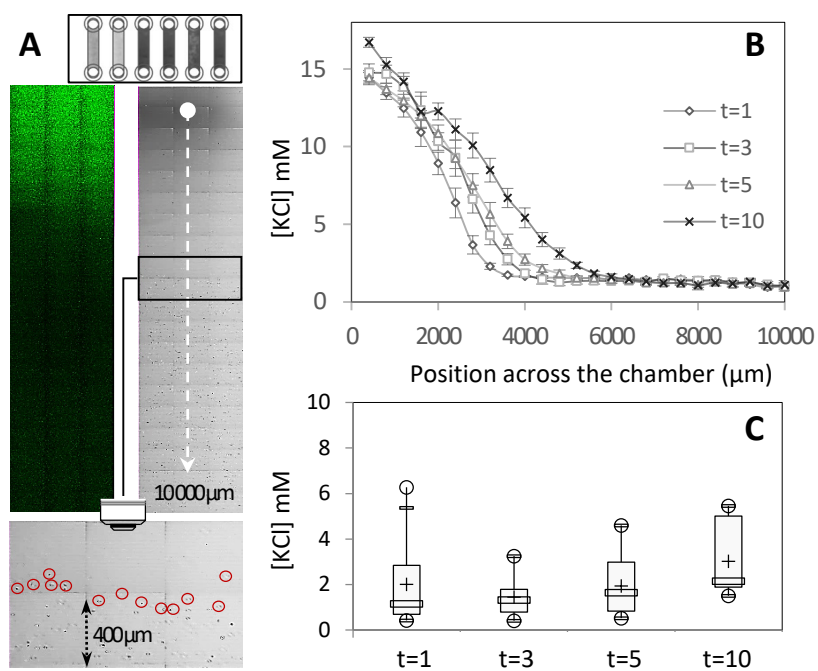
Comment citer ce document :

Galiana, E. (Auteur de correspondance), Cohen, C., Thomen, P., Etienne, C., Noblin, X. (2019). Guidance of zoospores by potassium gradient sensing mediates aggregation. *Journal of the Royal Society Interface*, 16 (157), 1-45. , DOI : 10.1098/rsif.2019.0367

**FIGURE 3**

Comment citer ce document :

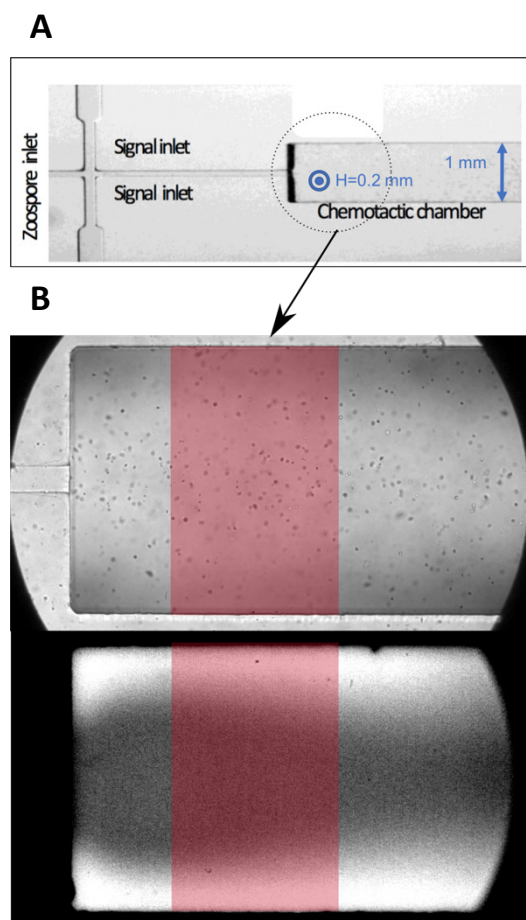
Galiana, E. (Auteur de correspondance), Cohen, C., Thomen, P., Etienne, C., Noblin, X. (2019). Guidance of zoospores by potassium gradient sensing mediates aggregation. *Journal of the Royal Society Interface*, 16 (157), 1-45. , DOI : 10.1098/rsif.2019.0367

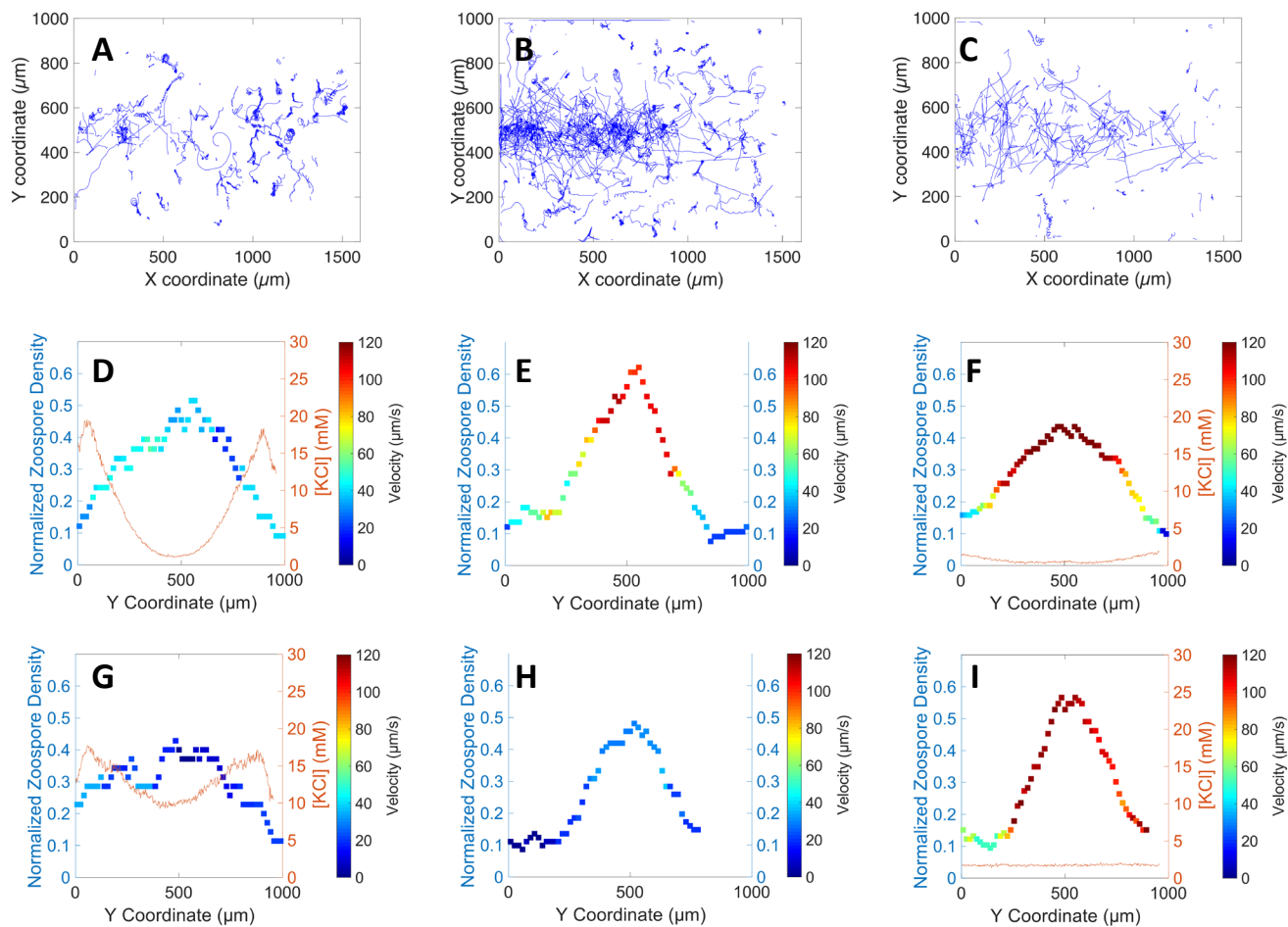


Comment citer ce document :

Galiana, E. (Auteur de correspondance), Cohen, C., Thomen, P., Etienne, C., Noblin, X. (2019). Guidance of zoospores by potassium gradient: a gradient that mediates aggregation. *Journal of the Royal Society Interface*, 16 (157), 1-45. , DOI : 10.1098/rsif.2019.0367

**FIGURE 4**





Comment citer **FIGURE 6**

Galiana, E. (Auteur de correspondance), Cohen, C., Thomen, P., Etienne, C., Noblin, X. (2019). Guidance of zoospores by potassium gradient sensing mediates aggregation. *Journal of the Royal Society Interface*, 16 (157), 1-45. , DOI : 10.1098/rsif.2019.0367

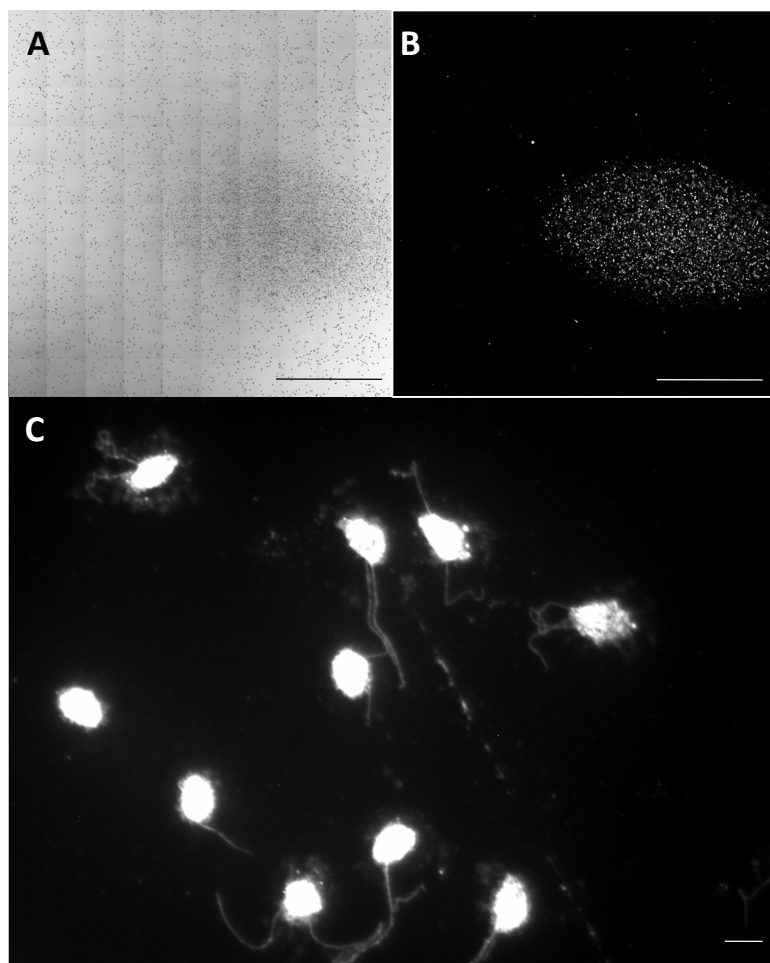
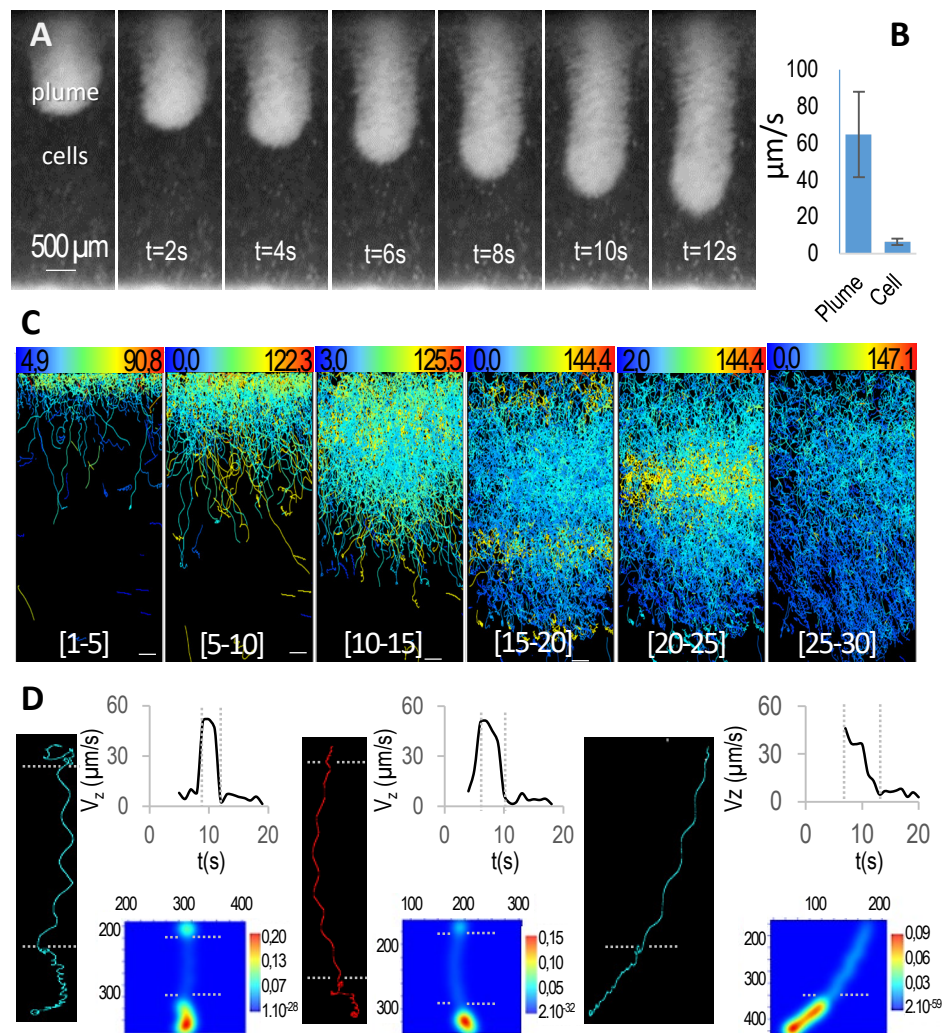


### Figure S1

Comment citer ce document :

Galiana, E. (Auteur de correspondance), Cohen, C., Thomen, P., Etienne, C., Noblin, X. (2019). Guidance of zoospores by potassium gradient sensing mediates aggregation. *Journal of the Royal Society Interface*, 16 (157), 1-45. , DOI : 10.1098/rsif.2019.0367



Comment citer cet article :

Galiana, E. (Auteur de correspondance), Cohen, C., Thomen, P., Etienne, C., Noblin, X. (2019). Guidance of zoospores by potassium gradient sensing mediates aggregation. *Journal of the Royal Society Interface*, 16 (157), 1-45. , DOI : 10.1098/rsif.2019.0367